Stress-Induced Tuning of Ultrasonic Additive Manufacturing Al-NiTi Composites

Ryan Hahnlen, Marcelo J. Dapino

Smart Vehicle Concepts Center, Department of Mechanical and Aerospace Engineering, The Ohio State University, Columbus, OH, USA, 43210

ABSTRACT

This paper addresses the development of active metal-matrix composites manufactured by Ultrasonic Additive Manufacturing (UAM), an emerging manufacturing process that allows the embedding of materials into seemingly solid metal components. In the UAM process, successive layers of metal tapes are ultrasonically bonded together at low temperatures to form a metal-matrix. Being a low-temperature process, UAM offers unprecedented opportunities to create metal components with embedded thermally-sensitive materials, such as shape memory alloys. In this study UAM is used to create composites with aluminum matrices and embedded NiTi ribbons. These composites exhibit tunability of both the coefficient of thermal expansion and natural frequencies. These effects are due to the phase-dependent modulus and transformation stresses developed by the prestrained NiTi phase. Since the embedded NiTi ribbons are constrained by the matrix, thermally-induced transformation from detwinned martensite to austenite will be accompanied by the generation of transformation stresses. The effect of transformation stress and changing phase of NiTi on thermally-induced strain is observed and modeled by combining strain matching algorithms with thermodynamic-based constitutive models. The composite model accurately describes effects due to changing NiTi modulus and strain recovery due to initial stress-induced martensitic volume fractions including a 200 $\mu\epsilon$ contraction with increasing temperature. The observed dynamic behaviors include up to a 16.6% increase in natural frequency at 100°C as compared to room temperature tests. No substantial increase in damping ratio was observed relative to solid aluminum.

Keywords: NiTi, metal-matrix composites, active composites, ultrasonic additive manufacturing, ultrasonic consolidation, variable natural frequency, coefficient of thermal expansion

1. INTRODUCTION

Shape Memory Alloys (SMAs) have unique properties due to a stress and temperature-dependent phase transformation between martensite, the low-temperature/high-stress phase, and austenite, the high-temperature/low-stress phase. While this transformation is most widely utilized for actuation purposes via the shape memory effect and high strain components through the super-elastic response of initially austenitic alloys, this research utilizes the phase-dependent modulus of SMAs and their ability to generate transformation stresses when they are initially prestrained. By embedding SMA elements within a metal-matrix composite, changes in elastic modulus allow for variable composite stiffness and matrix reinforcement while transformation stresses can create axial loads, all of which are utilized to create unique thermally-induced strain responses and tune the dynamic behavior of the composites. An SMA metal-matrix composite can be designed such that the stress that develops due to phase transformation and strain recovery can be utilized to offset the coefficient of thermal expansion (CTE) of the matrix. Additionally, by varying the stress in a composite structure, the dynamic response of the system can be drastically changed[1–4] creating a tunable component controlled by changes in temperature.

Composites in this research are constructed using Ultrasonic Additive Manufacturing (UAM), a rapid prototyping technology based on ultrasonic metal welding. In UAM, two workpieces are held together under a compressive load and ultrasonically vibrated relative to one another. The motion creates a friction-like action that disrupts surface oxides and shears surface asperities on a micro-scale creating nascent surfaces.[5,6] The

Further author information: (Send correspondence to M.J.D)
R.H.: E-mail: hahnlen.1@osu.edu, Telephone: 1-614-247-7480
M.J.D.: E-mail: dapino.1@osu.edu, Telephone: 1-614-688-3689

Behavior and Mechanics of Multifunctional Materials and Composites 2012,
edited by Nakhiah C. Goulbourne, Zoubeida Ounaies, Proc. of SPIE Vol. 8342, 83421J · © 2012 SPIE
CCC code: 0277-786X/12/$18 · doi: 10.1117/12.915582

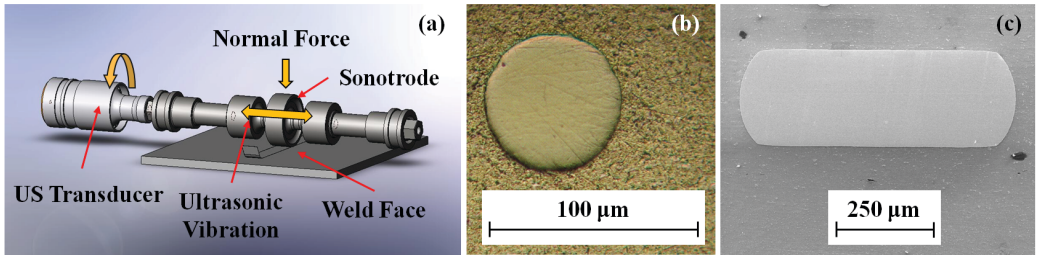

Figure 1. (a) In the UAM process, successive layers of metal tape are bonded together for creating metallic composites with seamlessly embedded materials and features; (b) Cross section of an Al-NiTi composite with 76 μm (0.003 in) diameter NiTi wire; (b) Cross section of an Al-NiTi composite with 254 μm by 762 μm (0.01 in by 0.03 in) NiTi ribbon.

compressive load applied to the pieces causes opposing clean metal surfaces to form metallic bonds, thus joining the two components. During UAM consolidation, illustrated in Fig. 1 (a), the ultrasonic vibrations are generated by piezoelectric transducers and transmitted to the workpieces through tuned waveguides and a rolling sonotrode which is specially textured to grip the top workpiece. The primary benefit of UAM is the low process temperatures. Pieces are consolidated at room temperature and macro-scale heating results in temperatures below 195°C.[7]

UAM makes it possible to embed thermally-sensitive materials such as SMAs, electroacitve PVDF, fiber optics, and electronic components within a metal-matrix[8–11] which would not be possible with other metal-matrix composite technologies that require melting or high temperature diffusion for construction. Embedding materials through UAM is accomplished by placing the materials to be embedded in between the workpieces being joined. Depending upon the size of the material to be embedded, pre-consolidation machining may be necessary to create a cavity to partially accommodate the material. During the welding phase, the ultrasonic vibrations of the workpieces and compressive stresses cause plastic deformation of the matrix material. The result is plastic flow of the matrix material around the embedded objects, creating close contact and mechanical interlocking between the composite components. To date, fibers ranging from 76 μm (0.003 in) to 381 μm (0.015 in) in diameter and ribbons up to 762 μm (0.030 in) wide, Fig. 1 (b) and (c), have been embedded without pre-consolidation machining, utilizing only plastic flow of the matrix.[7,12,13]

In this paper, the thermally-induced strain of Al-NiTi UAM composites is examined for development of a constitutive model for the composite system. The composites are also the subject of dynamic experiments to observe how natural frequency and damping ratio change as a function of temperature for different boundary conditions. The model developed from the strain behavior is utilized to describe the observed effects of transformation stress and phase transformation of the embedded NiTi elements.

2. METHODS

2.1 Composite Construction

Three Al-NiTi composites were constructed for thermomechanical testing. Each composite consists of four 152 μm (0.006 in) thick Al 3003-H18 tapes with NiTi ribbons embedded between the second and third tape. NiTi ribbons have 254 μm by 762 μm (0.01 in by 0.03 in) rectangular cross sections. Composite 1 has a single embedded ribbon while composites 2 and 3 each have two embedded ribbons. Prior to embedding, the ribbons were heated, inducing the martensite to austenite (M-A) transformation, to remove any previously induced detwinned martensite. The ribbons were allowed to cool and assumed to be embedded in their twinned martensitic state. The validity of this assumption is discussed in 3.1. Composites are consolidated on a sacrificial Al 3003-H18 baseplate which is machined away in post-consolidation processing. After consolidation, composites 1, 2, and 3 were machined to final dimensions to form beams with 5%, 15%, and 20% NiTi volume fractions, respectively. Final dimensions for each composite are summarized in Table 1.

2.2 Thermally-Induced Strain

To measure thermally-induced strain, each composite was placed in a thermal chamber with an Al 3003-H18 reference sample and cycled three times from 25 °C to 100 °C and allowed to cool. During thermal cycles, the

Table 1. Dimensions and NiTi content of Al-NiTi composites.

Composite	Number of Ribbons	Cross Sectional Area [mm^2]	Length [mm]	NiTi Volume Fraction
1	1	3.52	76.2	5%
2	2	2.54	74.0	15%
3	2	1.88	71.9	20%

strain of each composite was measured with a strain gage matched to aluminum alloys and the temperature of the composites was monitored with a thermocouple placed next to the strain gages.

Since the CTE of the reference sample is known, the strain signal from the reference sample was used to remove the thermal dependency of the strain gages from the composite strain signals. To determine the composite strain, the strain measured from the reference sample was subtracted from the strain measured from each composite and then the calculated thermal strain of the reference sample was added to the composite strain measurements:[14]

$$\epsilon_{comp} = \epsilon_{sig/comp} - \epsilon_{sig/ref} + \alpha_{ref} \times \Delta T. \tag{1}$$

Here, $\epsilon_{sig/comp}$ is the non-compensated strain signal from the composite, $\epsilon_{sig/ref}$ is the strain signal from the reference sample, α_{ref} is the CTE of the reference material[15] (23.2 ppm/°C), and ΔT is the change in temperature.

2.3 Dynamic Testing

The composites and an Al 3003 H-18 reference sample were subjected to dynamic testing. Dynamic tests consisted of applying a harmonic force to a clamping fixture while measuring displacement of the samples with a laser displacement sensor and the applied force with a piezoelectric load washer. Two fixtures were used for dynamic testing. The first fixture creates a cantilevered condition (C-F) consisting of a clamp on one end and leaving the other end of the sample free. When installing beams on the C-F fixture, total length was set at 34.93 mm (1.375 in) with displacement measurements taken at 31.8 mm (1.25 in) from the fixed end. The second fixture holds both ends of the composite fixed with clamped boundary conditions (C-C). The distance between each clamp is 38.10 mm (1.500 in) and displacement measurements were taken at the mid-span of the beams. Both fixtures were constructed from Al 3003-H18 and can be seen in Fig. 2.

For each boundary condition, the fixtures were attached to an electrodynamic shaker using a stinger that placed the fixtures and samples in a thermal chamber. Dynamic excitation consisted of 50 chirps over a range of 200 to 500 Hz for the C-F tests and 1500 to 3000 Hz for the C-C tests. Tests were conducted at nominal chamber temperatures of 24°C, 40°C, 60°C, 70°C, 90°C and 100°C in both heating and cooling sequences. Between each test, the thermal chamber was allowed to reach equilibrium to ensure that both the sample and fixture were at the same temperature before recording data. Temperature was monitored by a thermocouple attached to each fixture.

The frequency response function displacement per force was created using the average of the transfer functions from the 50 chirp excitations in each experiment. System natural frequencies and damping ratios were identified from the resonant peaks and half-power frequencies.

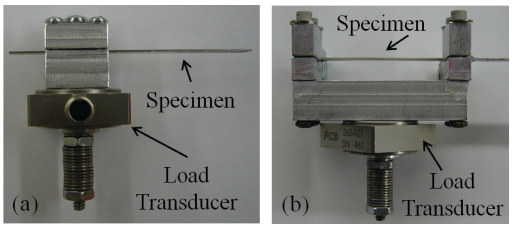

Figure 2. Composite fixtures for dynamic testing: (a) Clamped-Free (C-F) fixture; (b) Clamped-Clamped (C-C) fixture.

3. RESULTS AND DISCUSSION

3.1 Thermally-Induced Strain Behavior

The repeatable temperature versus strain plots, consisting of cycles 2 and 3, of each composites are shown in Fig. 3 (a)-(c). For each composite, the initial cycle is different than subsequent cycles. This initial behavior is believed to be due to residual detwinning and initial mechanical loading of the SMA elements from composite manufacturing. Similar effects have been observed in thermal cycling of constrained SMAs.[16] An in-depth analysis of this initial, non-repeatable behavior has been discussed in previous work.[7]

In all three composites there are two linear regions corresponding to the martensite and austenite phases of the embedded NiTi ribbons. While difficult to observe in composite 1, the effect becomes more pronounced as NiTi volume fraction increases as seen in the responses of composites 2 and 3. Since NiTi has a lower CTE than the Al matrix, the inclusion of NiTi elements will reduce the total composite CTE, α_{comp}, to varying degrees. The influence of the NiTi ribbons on the composite CTE is a function of their modulus, as holds true for a typical long-fiber reinforced composite:[17–19]

$$\alpha_{comp} = \frac{(1-\nu)(E_{Al})(\alpha_{Al}) + \nu(E_{NiTi})(\alpha_{NiTi})}{(1-\nu)(E_{Al}) + \nu(E_{NiTi})}, \tag{2}$$

where ν is the NiTi fiber volume fraction of the composite, E_{Al}, E_{NiTi}, α_{Al}, and α_{NiTi} are the elastic moduli and CTEs of Al and NiTi, respectively. At high temperatures, the modulus of the embedded NiTi increases, due to transformation to austenite, further reducing the total composite CTE. This results in a higher strain-temperature slope at low temperatures and a lower slope at high temperatures corresponding to the higher and lower composite CTEs.

Composite 2 has an additional behavior unique among all of the tested samples. Starting at approximately 50°C ($\Delta T = 25$°C) a negative strain-temperature slope is observed resulting in a contraction until approximately 55°C ($\Delta T = 30$°C) whereupon the composite resumes a linear strain-temperature relationship. On cooling, the recovered strain is introduced back into the composite over a temperature range of approximately 45°C to 40°C ($\Delta T = 20$°C to 15°C). This hysteretic behavior and strain recovery are characteristic of the shape memory effect of NiTi. Further, strain recovery is only possible if there is a prestrain or stress-induced martensite present in the embedded NiTi ribbons.

To model the thermal strain response of the composites, a strain matching method, similar to that presented by Sittner[20–22] for SMA-epoxy based composites, was employed. The original model utilizes a phenomenological basis for the transformation of the embedded SMA fibers and splits the transformation strain into the initial prestrain, ϵ^c, the strain recovered through transformation of the SMA, ϵ^t, and considers elastic, ϵ^{el}, and thermal, ϵ^{th}, strains in the SMA and matrix:

$$\epsilon_{NiTi} = \epsilon^{el}_{NiTi} + \epsilon^{th}_{NiTi} + \epsilon^t = \epsilon_{Al} = \epsilon^{el}_{Al} + \epsilon^{th}_{Al} + \epsilon^c. \tag{3}$$

The strain for each component is expanded:

$$\epsilon_{NiTi} = \frac{1}{E_{NiTi}}\left(\Delta\sigma_{NiTi}\right) + \alpha_{NiTi}\left(\Delta T\right) + \epsilon_L \xi_s \tag{4}$$

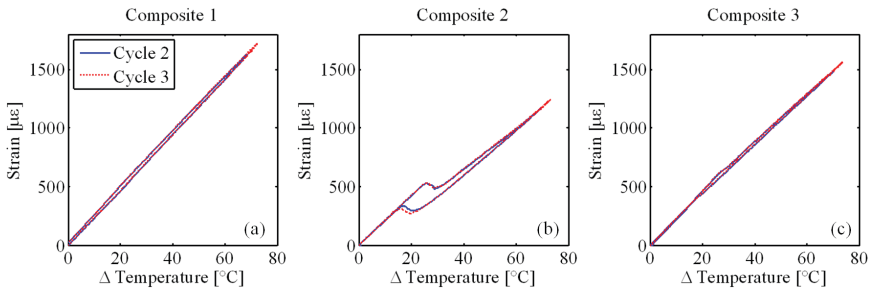

Figure 3. Temperature versus strain plots for the second and third thermal cycles of Al-NiTi: (a) composite 1; (b) composite 2; (c) composite 3.

and

$$\epsilon_{Al} = \frac{1}{E_{Al}} \left(\Delta\sigma_{Al}\right) + \alpha_{Al} \left(\Delta T\right) + \epsilon_L \xi_{so} \tag{5}$$

where $\Delta\sigma$ is the change in total stress from the initial state, ξ_s is the stress-induced martensitic volume fraction, ξ_{so} is the initial stress-induced martensitic volume fraction, and ϵ_L is the maximum recoverable strain of NiTi. By moving the initial prestrain term in (3), the NiTi strain can be expressed as an alternative constitutive equation including elastic, thermal, and transformation strain terms:

$$\epsilon_{NiTi} = \frac{1}{E_{NiTi}} \left(\Delta\sigma_{NiTi}\right) + \alpha_{NiTi} \left(\Delta T\right) + \epsilon_L \left(\xi_s - \xi_{so}\right). \tag{6}$$

The corresponding alternative matrix strain equation now accounts for only thermo-elastic strains, an assumption that is valid as long as the matrix does not undergo plastic deformation:

$$\epsilon_{Al} = \frac{1}{E_{Al}} \left(\Delta\sigma_{Al}\right) + \alpha_{Al} \left(\Delta T\right). \tag{7}$$

In the thermally-induced strain tests, no external load was applied; the composite is allowed to freely expand or contract as the temperature changes. As such, force balance is used to obtain the stress in the Al matrix in terms of NiTi stress:

$$\begin{aligned} \sigma_{NiTi} A_{NiTi} + \sigma_{Al} A_{Al} &= 0 \\ \sigma_{Al} &= -\frac{A_{NiTi}}{A_{Al}} \sigma_{NiTi} \\ \sigma_{Al} &= \frac{-\nu}{(1-\nu)} \sigma_{NiTi}, \end{aligned} \tag{8}$$

where A_{NiTi} and A_{Al} are the cross sectional areas of the NiTi ribbons and Al matrix, respectively. The variable change from cross sectional area to fiber volume fraction can be made because the NiTi ribbons provide long-fiber reinforcement of the Al matrix and the lengths of both components are equal, $L_{NiTi} = L_{Al}$. Thus, a ratio of cross sectional areas for these composites is equal to a ratio of fiber and matrix volume fraction. Assuming zero initial stress, the stress in the ribbons can be obtained as a function of temperature, material properties, volume fraction, and NiTi transformation terms by substituting (8) into (7), equating to (6), and solving for σ_{NiTi}:

$$\sigma_{NiTi} = \frac{\left(\alpha_{Al} - \alpha_{NiTi}\right)\left(\Delta T\right)}{\frac{1}{E_{NiTi}} + \frac{1}{E_{Al}} \frac{\nu}{(1-\nu)}} - \frac{\epsilon_L \left(\xi_s - \xi_{so}\right)}{\frac{1}{E_{NiTi}} + \frac{1}{E_{Al}} \frac{\nu}{(1-\nu)}}. \tag{9}$$

This equation has two components: the first is the thermo-elastic component which any composite exhibits if a CTE mismatch exists between the fibers and matrix; the second is due to the transformation-induced strain recovery of NiTi if it was embedded in a detwinned state ($\xi_{so} \neq 0$). If the embedded NiTi elements are not prestrained before construction, the thermo-elastic stress component is non-linear due to the change in modulus as the NiTi ribbons transform between martensite and austenite. In addition to a variable NiTi modulus, the modulus of the Al matrix also varies with temperature, decreasing as temperature increases. Once the NiTi stress is calculated it can be used in (6) to determine total composite strain:

$$\epsilon_{comp} = \epsilon_{NiTi} = \frac{1}{E_{NiTi}} \left[\frac{\left(\alpha_{Al} - \alpha_{NiTi}\right)\left(\Delta T\right)}{\frac{1}{E_{NiTi}} + \frac{1}{E_{Al}} \frac{\nu}{(1-\nu)}} - \frac{\epsilon_L \left(\xi_s - \xi_{so}\right)}{\frac{1}{E_{NiTi}} + \frac{1}{E_{Al}} \frac{\nu}{(1-\nu)}} \right] + \alpha_{NiTi} \left(\Delta T\right) + \epsilon_L \left(\xi_s - \xi_{so}\right). \tag{10}$$

The composites were assumed to be consolidated in a twinned martensite state, having an initial stress-induced volume fraction of zero. As such, the initial models for thermally-induced strain do not include the transformation strain recovery components and (10) becomes:

$$\epsilon_{comp} = \epsilon_{NiTi/TE} = \frac{1}{E_{NiTi}} \left[\frac{\left(\alpha_{Al} - \alpha_{NiTi}\right)\left(\Delta T\right)}{\frac{1}{E_{NiTi}} + \frac{1}{E_{Al}} \frac{\nu}{(1-\nu)}} \right] + \alpha_{NiTi} \left(\Delta T\right). \tag{11}$$

If the zero prestrain assumption is maintained, the strain calculation is completed by finding the elastic modulus of the NiTi ribbons and the Al matrix as a function of temperature. The elastic modulus of the Al matrix is varied linearly using modulus values at different temperatures as found in the literature.[15] The elastic modulus of NiTi is found through a rule of mixtures between its martensite and austenite phases:

$$E_{NiTi} = E_A + \xi \left(E_M - E_A\right) \tag{12}$$

where E_A and E_M are the elastic moduli of austenite and martensite, respectively, and ξ is the total martensitic volume fraction. The martensitic volume fraction only decreases over the range defined by the austenite start and finish temperatures as composite temperature increases. Conversely, increasing volume faction only occurs over the martensitic start and finish temperatures while the composite temperature is decreasing. The austenite and martensite transformation temperatures are assumed to vary linearly with stress:[23–26]

$$A_s^\sigma = A_s + \sigma_{NiTi}/C_A \tag{13}$$

$$A_f^\sigma = A_f + \sigma_{NiTi}/C_A \tag{14}$$

$$M_s^\sigma = M_s + \sigma_{NiTi}/C_M \tag{15}$$

$$M_f^\sigma = M_f + \sigma_{NiTi}/C_M \tag{16}$$

where A_s, A_f, M_s, and M_s are the respective austenite and martensite start and finish temperatures at zero stress; C_A and C_M are the stress influence coefficients, often assumed to be equal.[26] For the NiTi ribbons used in this study, the transition temperatures were found through electrical resistance tests and differential scanning calorimetry; the stress influence coefficient was found from blocked force experiments. Blocked force experiments only provide a value for C_A. Attempts were made to find C_M through iso-thermal load cycles, however it is not possible to produce a super-elastic stress-strain loop with the given alloy. At temperatures above A_f, the ribbons failed before the transformation to stress-induced martensite was completed. As such, the model presented assumes $C_M = C_A$. Experimentally obtained properties can be seen in Table 2. Even in the thermo-elastic case, the increasing NiTi stress due to thermal mismatch of the NiTi ribbons and Al matrix necessitates using the stress-modified transformation temperatures. In the case of an initial stress-induced martensitic volume fraction ($\xi_{so} \neq 0$) the transformation temperatures will increase further due to additional stresses from SMA strain recovery.

The martensitic volume fractions are found through equations based upon the Brinson[23] and Liang and Rogers[24, 25] constitutive SMA models. For the martensite to austenite (M-A) transformation the volume fraction is:

$$\xi = \frac{\xi_0}{2}\left(\cos\left[a_A\left(T - A_s^\sigma\right)\right] + 1\right), \tag{17}$$

where

$$a_A = \frac{\pi}{A_f - A_s}. \tag{18}$$

For the austenite to martensite (A-M) transformation the total volume fraction is calculated using:

$$\xi = \frac{1 - \xi_0}{2}\cos\left[a_M\left(T - M_f^\sigma\right)\right] + \frac{1 + \xi_0}{2}, \tag{19}$$

where

$$a_M = \frac{\pi}{M_s - M_f}. \tag{20}$$

The stress-modified temperatures were initially found using the thermo-elastic stresses considering martensitic and austenitic phases of the embedded NiTi ribbons. The thermo-elastic stresses were plotted on the stress-temperature phase diagram and the locations of intersection with the stress-dependent transformation temperatures provide the stresses and temperatures when both the M-A and A-M transformations start and finish. The stress-temperature relationship is illustrated for a single thermal cycle in Fig. 4 (a). Initially, the stress will increase linearly as governed by the martensitic thermo-elastic equation until the temperature reaches

A_s^σ. Between A_s^σ and A_f^σ, the stress will change due to the changing modulus of NiTi, increasing to coincide with the austenitic thermo-elastic stress. Upon cooling from temperatures beyond A_f^σ, the stress will decrease linearly following the austenitic thermo-elastic equation until M_s^σ. Between M_s^σ and M_f^σ, the stress will decrease, ultimately coinciding with the martensitic thermo-elastic stress at M_f^σ and from there it will decrease linearly to zero.

The thermo-elastic strains were modeled for each composite using the material and composite properties found in Table 2. The model output can be seen for composites 1-3 in Fig. 5 (a)-(c), respectively. For composites 1 and 3 the strain model closely matches the strain observed in the experiments, including a high and low temperature linear region and a small amount of hysteresis. However, the model does not describe the negative strain-temperature regions observed in composite 2. This confirms that the zero prestrain assumption is not valid when considering composite 2 and there is residual prestrain that was induced by the rolling action of the sonotrode during construction. The amount of stress-induced martensite is not directly known but can be determined by observing the amount of strain recovered as the NiTi ribbons go through the M-A transformation.

The strain recovery region observed in composite 2 is consistent over multiple cycles. Because of this, the transformation is assumed to recover and induce a repeatable amount of stress-induced martensite as the composite is heated and cooled. To this end, an assumption is made that $\xi_s = \xi_{so} \times \xi$ where ξ is found from (17) and (19) for purposes of calculating composite strain. By taking the average strain of the rising and falling high temperature linear regions at T=65°C, a temperature slightly beyond the M-A transformation region, and subtracting the modeled thermo-elastic strain for composite 2 at 65°C, the total composite recovery strain, $\epsilon_{NiTi/X}$, was estimated as 200 $\mu\epsilon$. To calculate the initial stress-induced volume fraction from the total observed strain recovery, the thermo-elastic strain component from (11) is subtracted from the total strain component (10),

$$\epsilon_{NiTi/total} - \epsilon_{NiTi/TE} = \epsilon_{NiTi/X} = \frac{1}{E_{NiTi}} \left(\sigma_{NiTi/X}\right) + \epsilon_L \left(\xi_s - \xi_{so}\right), \tag{21}$$

where $\sigma_{NiTi/X}$ is equal to the second term of (9). Considering $E_{NiTi} = E_A$ and $\xi_s = 0$ when the NiTi ribbon is

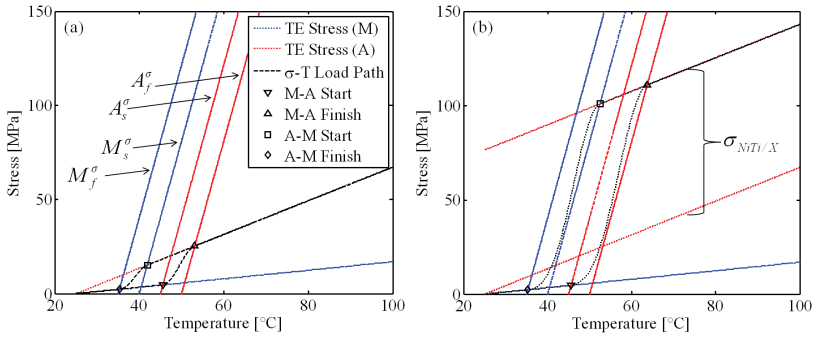

Figure 4. Stress-temperature phase diagram for NiTi and overlaid stress-temperature load paths for composite 2 assuming: (a) $\xi_{so} = 0$; (b) $\xi_{so} = 1.9\%$.

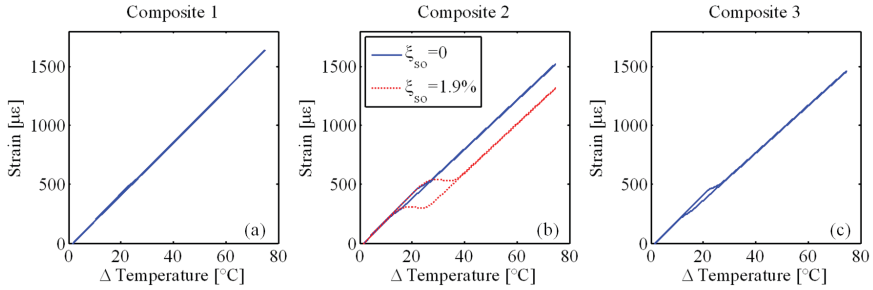

Figure 5. Thermally-induced strain models for Al-NiTi: (a) composite 1; (b) composite 2; (c) composite 3.

Table 2. Material properties used for composite stiffnesses model. Unless cited, values were found experimentally.

Property	Description	Value
E_A[27]	Austenite elastic modulus	83 GPa
E_M	Martensite elastic modulus	17.9 GPa
$E_{Al}(24\,^\circ\mathrm{C})$[15]	Al 3003 elastic modulus at 24 °C	68.3 GPa
$E_{Al}(100\,^\circ\mathrm{C})$[15]	Al 3003 elastic modulus at 100 °C	65.5 GPa
α_{Al}[15]	Al 3003 CTE	23.2 $\mu\epsilon/^\circ$C
α_{NiTi}[26]	NiTi CTE	10 $\mu\epsilon/^\circ$C
M_f	Martensite finish temperature	35°C
M_s	Martensite start temperature	40°C
A_s	Austenite start temperature	45°C
A_f	Austenite finish temperature	50°C
C_M, C_A	Stress influence coefficient	8.1 MPa
ϵ_L	Maximum recovery strain	-6%

austenitic,

$$\epsilon_{NiTi/X} = \frac{1}{E_{NiTi}}\left[\frac{-\epsilon_L\left(\xi_s - \xi_{so}\right)}{\frac{1}{E_{NiTi}} + \frac{1}{E_{Al}}\frac{\nu}{(1-\nu)}}\right] + \epsilon_L\left(\xi_s - \xi_{so}\right) = -\epsilon_L\xi_{so}\left[1 - \frac{1}{1 + \frac{E_A}{E_{Al}}\frac{\nu}{(1-\nu)}}\right]. \tag{22}$$

Using 200 $\mu\epsilon$ for $\epsilon_{NiTi/X}$, the initial stress-induced martensitic volume fraction is found to be 1.9%. For small amounts of stress-induced martensite, the associated strain recovery is possible without causing failure of the NiTi ribbon, Al matrix, or NiTi/Al interface. At the calculated prestrain, the NiTi stress-temperature load path is shown on the phase diagram in Fig. 4 (b). Compared to the load path for the thermo-elastic response in Fig. 4 (a), the transformation to austenite is accompanied by higher stress on the NiTi ribbons, thereby further increasing the transformation temperatures. After the M-A transformation is complete, the stress increases linearly as given by the austenitic thermo-elastic equation previously noted. The red dashed line in Fig. 5 (b) shows the thermally-induced strain model for composite 2 including the transformation strain component. With the inclusion of the transformation strain term, the model closely matches the experimental data and exhibits the negative strain-temperature slope region originally observed.

3.2 Dynamic Behavior

Results from the C-F and C-C dynamic tests are compiled in Tables 3 and 4, respectively. The change in natural frequency, ω_n, and damping ratio, ζ, relative to their respective room temperature values are shown in Fig. 6 (a) and (b) for the C-F boundary condition and in Fig. 6 (c) and (d) for the C-C boundary condition. The percent change is used to normalize the results with respect to sample geometry since cross sectional areas were varied to obtain specific NiTi volume fractions. Further, solid trend lines in the figure represent the average of the rising and falling temperature values for each nominal temperature test point. While there is likely hysteresis in the responses of these properties due to the offset martensitic and austenitic transition temperatures, the temperature resolution for these tests was not sufficient to observe such effects.

Table 3. Natural frequency and damping ratios of samples from C-F dynamic tests.

Temp [°C]	Natural Frequency [Hz]				Damping Ratio ($\times 10^{-3}$)			
	Solid Al	Comp 1	Comp 2	Comp 3	Solid Al	Comp 1	Comp 2	Comp 3
24	414.1	362.5	283.6	339.1	5.8	3.5	8.5	9.8
40	413.3	361.7	282.8	338.3	10.4	4.7	11.4	7.1
60	411.7	360.9	285.2	339.1	8.0	4.8	5.6	6.4
70	410.9	360.2	285.2	339.1	8.9	6.4	5.9	8.4
90	409.4	359.4	284.4	337.5	9.9	7.5	8.9	6.8
100	408.6	357.8	283.6	336.7	8.7	5.2	14.4	4.8

Table 4. Natural frequency and damping ratios of samples from C-C dynamic tests.

Temp [°C]	Natural Frequency [Hz]				Damping Ratio ($\times 10^{-3}$)			
	Solid Al	Comp 1	Comp 2	Comp 3	Solid Al	Comp 1	Comp 2	Comp 3
24	2275	1939	1806	1850	4.3	6.0	6.9	7.3
40	2264	1941	1828	1859	5.4	7.4	7.8	8.1
60	2252	1974	1988	1959	7.4	9.4	10.5	13.5
70	2239	1984	2048	1989	7.0	8.9	7.6	11.0
90	2219	1995	2089	2013	6.7	9.4	8.8	12.0
100	2217	2003	2106	2028	6.7	9.9	9.0	10.2

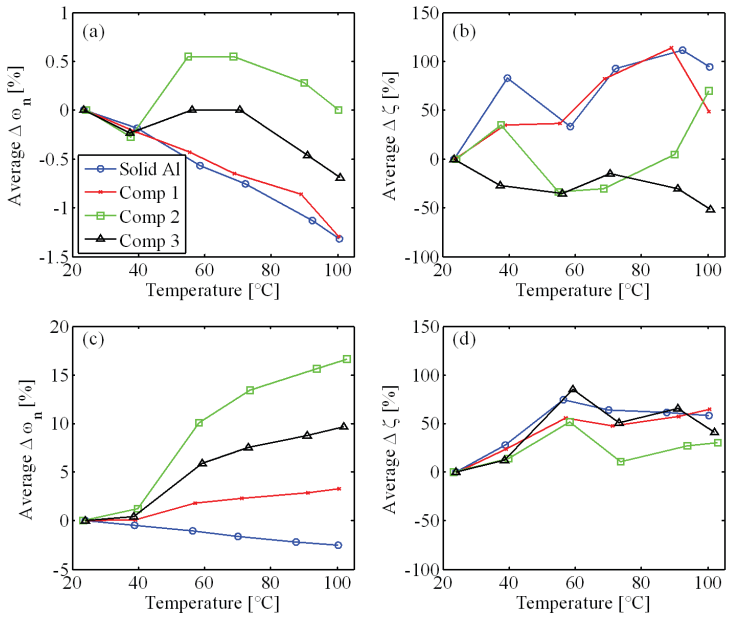

Figure 6. Change in dynamic behavior as a function of temperature: (a) C-F test relative $\Delta\omega_n$; (b) C-F test relative $\Delta\zeta$; (c) C-C test average relative $\Delta\omega_n$; (d) C-C test average relative $\Delta\zeta$.

For the C-F boundary condition, the Al sample exhibits a linear decrease in natural frequency as temperature increases due to a drop in modulus, subsequently decreasing the samples bending stiffness. The largest relative change in natural frequency was -1.32% at 100°C. Composite 1 shows a similar decrease in natural frequency, reaching a relative change of -1.29% at 100°C. At a temperature of 60°C and above, composite 1 has a smaller relative decrease in natural frequency than the solid Al sample due to the M-A transformation of the embedded NiTi ribbons; as a result of the transformation and higher modulus of the austenite phase, the loss in stiffnesses of the Al matrix due to increasing temperature is partially offset. This effect is expected to increase as NiTi volume fraction increases.

Composites 2 and 3 show a non-linear relationship between temperature and natural frequency. From Fig. 6 (a) both composites show a change in natural frequency similar to the solid Al sample and composite 1. However, at 60°C composite 2 shows an increase in natural frequency relative to room temperature while composite 3 completely recovers any loss in natural frequency due to the drop in modulus of the Al matrix. Starting at 70°C, both composites continue a linear decrease in natural frequency with increasing temperature that is similar in rate to the Al sample and composite 1. The initial increase in natural frequency is due to the transformation of the embedded NiTi ribbons; at 60°C, the increase in bending stiffness of the ribbons is greater than the decreasing stiffness of the matrix due to heating. The effect is relatively small because while the change in NiTi modulus is significant, bending stiffness is also a function of the moment of inertia of all components. The small cross section of the ribbons as compared to the Al matrix combined with their placement near the neutral axis of the composite results in a relatively minute effect.

It is noted that composite 2, with 15% NiTi, has a net positive change in natural frequency at mid-range temperatures and no change in natural frequency at 100°C while the natural frequency of composite 3, with 20% NiTi, never exceeds the natural frequency recorded at room temperature. An examination of composite 2 showed that near the clamped end of the composite, total thickness was greater than expected, 0.686 mm (0.027 in) rather than 0.610 mm (0.024 in), indicating the presence of additional baseplate material that was not fully removed. This extra material offsets the NiTi ribbons from the neutral axis causing the transformaton to austenite to have a larger effect on the composite bending stiffness than if it were embedded at the neutral axis. This concept could be used to create composites with large natural frequency shifts through strategic placement of embedded SMAs rather than increasing the total SMA volume fraction.

The damping ratios of all composites are similar in magnitude to that of the solid Al sample. Both the solid Al sample and composite 1 have similar increases in damping ratio with increasing temperature. Composite 2 shows an initial increase in damping ratio with temperature but exhibits a sharp decrease corresponding with the M-A transformation at 60°C. From 60°C on, the damping ratio increases with temperature. Composite 3 exhibits consistently lower damping ratios relative to the room temperature value at all elevated temperatures. When considering composite materials, the damping ratios are generally assumed to be higher than that of isotropic materials. This is attributed to friction between laminate layers, the matrix and fiber, or damage to the composite.[28,29] However, in this study it appears that UAM composites do not exhibit this characteristic of composite materials.

Dynamic test results from the C-C boundary condition show a significantly different composite behavior than the C-F boundary condition. While the solid Al sample exhibits a linear decrease in natural frequency with increasing temperature, all three Al-NiTi composites exhibit increasing natural frequency with increasing temperature. Due to the C-C boundary condition, the lower CTE of the composites relative to the Al 3003 fixture causes a tensile stress to develop thereby creating an increase in natural frequency as temperature increases. According to the zero prestrain assumption, composites 1, 2, and 3 should have increasing changes in natural frequency due to progressively higher NiTi fiber volume fractions creating progressively lower composite CTEs. The lower CTEs cause greater stresses to develop as temperature increases due to CTE mismatch between the sample and fixture. As observed by the thermally-induced strain study, composite 2 has a non-negligible prestrain and a strain contraction as it is heated to 100°C. As a result, composite 2 generates larger tensile stresses in the C-C boundary condition than composite 3 even though it has a smaller NiTi volume fraction. This is reflected in the larger increase in natural frequency that composite 2 exhibits at temperatures above 60°C, up to 16.6%. Composite 1 and 3 have maximum increases in natural frequency of 3.3% and 9.6%, respectively, while the solid Al sample exhibits a change of −2.5%. In addition to the maximum relative increase in natural frequency, all composites have a sharp increase between 40°C and 60°C. This corresponds to the phase transformation of the embedded NiTi elements as the austenitic composites have a lower composite CTE, thereby creating higher tensile stresses. Similar to the results for the C-F boundary condition, the composites have damping ratios similar in magnitude to the solid Al sample. However, contrary to the C-F boundary condition, all samples have increasing damping ratios with increasing temperatures.

Continuing work is focused on utilizing the model developed to describe thermally-induced composite strain to determine the stresses on the composites for the C-C boundary condition. While differential thermal expansion between the fixture and composites was the main contribution to the shifting natural frequency, the behavior of composite 2 suggests that prestrain can create much more significant changes. With higher initial stress-induced volume fractions, larger internal stresses can be generated with future composites creating tunable dynamic systems which exhibit a broader frequency range.

4. SUMMARY

In this research, UAM has been used to create composites with shape memory NiTi embedded within an Al matrix. The composites display unique behaviors due to a combination of NiTi fiber volume fraction and prestrain which creates residual stress-induced martensite. Thermally-induced strain, natural frequency, and damping ratio were measured for three composite with 5%, 15%, and 20% NiTi as well as a solid Al reference sample.

In studying the thermally-induced strain, it was found that embedding zero prestrain NiTi creates a composite system with unique low and high temperature CTEs and a small hysteresis region corresponding to the transformation between the martensitic and austenitic phases. As volume fraction increases, these effects increase in magnitude. When the embedded NiTi element has a non-zero prestrain, it recovers the induced strain causing a net contraction of the composite over a finite increasing temperature range. This was observed in the behavior of composite 2 which contracts 200 $\mu\epsilon$ when heated from 50°C to 60°C. A model was created for the thermally-induced strain behavior by equating the constitutive strain relations of the embedded NiTi ribbons and Al matrix. Using an SMA transformation model, based upon the Brinson and Liang and Rogers models, to account for NiTi prestrain and phase-dependent modulus, the composite model output closely matches the behavior observed in all three composites.

Two different boundary conditions were considered in dynamic tests. For the C-F boundary condition, composites mitigated the decrease in natural frequency with increasing temperature exhibited by the solid Al reference sample. Composite 2 demonstrates the largest change, a 0.6% increase in natural frequency starting at 60°C relative to room temperature, due to the transformation of the embedded NiTi ribbons and their location slightly offset from the composite neutral axis. By placing SMA elements further from the composite neutral axis, it may be possible to create larger increases in natural frequency with smaller volume fractions. In the C-C boundary condition, all composites exhibited significant increases in natural frequency with temperature. Composite 2 has the largest increase in natural frequency, 16.6% at 100°C relative to room temperature, due to the additional tensile stresses generated by the transformation of the embedded prestrained NiTi elements. By increasing prestrain in the embedded elements, natural frequency shifts can be substantially increased. In both boundary conditions, the damping ratios of the composites were found to be similar to that of the solid Al sample. This indicates that neither the composite nature of the specimens nor stress-induced martensitic transformations of the embedded NiTi ribbons cause a substantial change in damping properties over the parent matrix material.

This paper enhances the understanding of the coupled thermomechanical behavior of SMA-Al composites. With the presented model, the behaviors can be accurately modeled for different volume fractions, prestrain levels, and boundary conditions allowing for the design of components with advanced capabilities such as thermal strain invariance, solid-state actuation, tunable natural frequencies, and stiffness control. Continuing work is focused on utilizing the developed model to design composites with highly prestrained and strategically located SMA elements to achieve greater control over the thermally-induced strain and variable dynamic properties.

ACKNOWLEDGMENTS

The authors would like to acknowledge Mark Norfolk, Matt Short, and Karl Graff from the Edison Welding Institute for their assistance and use of UAM equipment. The NiTi ribbon was provided by Nitinol Devices and Components. Financial support for this research was provided by the member organizations of the Smart Vehicle Concepts Center (www.SmartVehicleCenter.org), a National Science Foundation Industry/University Cooperative Research Center (I/UCRC). R.H. was partially supported by a Smart Vehicle Concepts Graduate Fellowship.

REFERENCES

[1] Parlinska, M., Clech, H., Balta, J. A., Michaud, V., Bidaux, J. E., Manson, J. A., and Gotthardt, R., "Adaptive composites with embedded shape memory alloys," *Journal de Physique IV - Proceedings* **11**, 197–204 (2001).

[2] Parlinska, M., Balta, J. A., Michaud, V., Bidaux, J. E., Manson, J. A., and Gotthardt, R., "Vibrational response of adaptive composites," *Journal de Physique IV - Proceedings* **11**, 129–134 (2001).

[3] Bidaux, J. E., Manson, J. A. E., and Gotthardt, R., "Active modification of the vibration frequencies of a polymer beam using shape-memory-alloy fibres," *Third Conference on Intelligent Materials and Third European Conference on Smart Structures and Materials*, 517–522 (1996).

[4] Friend, C. M. and Mattey, C. R. D., "Active strain-energy tuning of low actuator-fraction shape-memory alloy (SMA) hybrid composites," *Materials Science and Engineering A* **273-275**, 799–803 (1999).

[5] De Vries, E., *Mechanics and Mechanisms of Ultrasonic Metal Welding*, PhD thesis, The Ohio State University, Columbus, OH (2004).
[6] Graff, K., [*New Developments in Advanced Welding*], Woodhead Publishing Limited, Cambridge, 241–296 (2005).
[7] Hahnlen, R. and Dapino, M., "Performance and modeling of active metal-matrix composites manufactured by ultrasonic additive manufacturing," *Proc. SPIE 7979* (2011).
[8] Siggard, E., *Investigative Research into the Structural Embedding of Electrical and Mechanical Systems using Ultrasonic Consolidation*, Master's thesis, Utah State University, Logan, UT (2007).
[9] Kong, C. and Soar, R., "Fabrication of metal-matrix composites and adaptive composites using ultrasonic consolidation process," *Materials Science and Engineering A* **412**, 12–18 (2005).
[10] Kong, C., Soar, R., and Dickens, P., "Ultrasonic consolidation for embedding SMA fibres within aluminium matrices," *Composite Structures* **66**, 421–427 (2004).
[11] Masurtschak, S. and Harris, R. A., "Enabling techniques for secure fibre positioning in ultrasonic consolidation for the production of smart material structures," *Proc. SPIE 7981* (2010).
[12] Hahnlen, R. and Dapino, M., "Active metal-matrix composites with embedded smart materials by ultrasonic additive manufacturing," *Proc. SPIE 7645* (2010).
[13] Hahnlen, R., Dapino, M., Short, M., and Graff, K., "Aluminum-matrix composites with embedded Ni-Ti wires by ultrasonic consolidation," *Proc. SPIE 7290* (2009).
[14] Lanza di Scalea, F., "Measurement of thermal expansion coefficients of composites using strain gauges," *Experimental Mechanics* **328**(4), 233–241 (1998).
[15] Kaufman, J., ed., [*Properties of Aluminum Alloys: Tensile, Creep, and Fatigue Data at High and Low Temperatures*], The Aluminum Association, Inc. and ASM International (1999).
[16] Vokoun, D., Kafka, V., and Hu, C., "Recovery stresses generated by NiTi shape memory wires under different constrain conditions," *Smart Materials and Structures* **12**, 680–685 (2003).
[17] Clyne, T. and Withers, P., [*An Introduction to Metal Matrix Composites*], Cambridge University Press, Cambridge, 12–14 (1993).
[18] Staab, G., [*Laminar Composites*], Butterworth-Heinemann, Boston, 92 (1999).
[19] Schapery, R. A., "Thermal expansion coefficients of composite materials based on energy principles," *Journal of Composite Materials* **2**(3), 380–404 (1968).
[20] Sittner, P., Michaud, V., and Schrooten, J., "Modeling and material design of SMA polymer composites," *Materials Transactions* **43**(5), 984–993 (2002).
[21] Sittner, P. and Stalmans, R., "Developing hybrid polymer composites with embedded shape-memory alloy wires," *JOM* **52**(10), 15–20 (2000).
[22] Sittner, P., Stalmans, R., and Tokuda, M., "An algorithm for prediction of the hysteretic responses of shape memory alloys," *Smart Materials and Structures* **9**(4), 452–465 (2000).
[23] Brinson, L., "One dimensional constitutive behavior of shape memory alloys," *Journal of Intelligent Material Systems and Structures* **4**(2), 229–242 (1993).
[24] Liang, C. and Rogers, C. A., "One-dimensional thermomechanical constitutive relations for shape memory materials," *Journal of Intelligent Material Systems and Structures* **1**, 207–234 (1990).
[25] Liang, C. and Rogers, C. A., "One-dimensional thermomechanical constitutive relations for shape memory materials," *Journal of Intelligent Material Systems and Structures* **8**, 285–302 (1997).
[26] Lagoudas, D., [*Shape Memory Alloys*], Science and Business Media, LLC, New York (2008).
[27] Johnson Matthey, "Nitinol technical specifications: Transformation, physical, electrical, magnetic and mechanical." jmmedical.com (2011).
[28] Chandra, R., Singh, S. P., and Gupta, K., "Damping studies in fiber-reinforced composites - a review," *Composite Structures* **49**, 41–51 (1999).
[29] Hwang, S. J. and Gibson, R. F., "The use of strain energy-based finite element techniques in the analysis of various aspects of damping of composite materials and structures," *Journal of Composite Materials* **26**(17), 2585–2605 (1992).